

Dissecting the broad-band emission from γ -ray blazar PKS 0735+178 in search of neutrinos

Raj Prince¹, Saikat Das², Nayantara Gupta³, Pratik Majumdar⁴ and Bożena Czerny¹

¹Center for Theoretical Physics, Polish Academy of Sciences, Al. Lotnikow 32/46, PL-02-668 Warsaw, Poland

²Center for Gravitational Physics and Quantum Information, Yukawa Institute for Theoretical Physics, Kyoto University, Kyoto 606-8502, Japan

³Astronomy & Astrophysics Group, Raman Research Institute, C.V. Raman Avenue, Sadashivanagar, Bangalore 560080, Karnataka, India

⁴Saha Institute of Nuclear Physics, a CI of Homi Bhabha National Institute, Kolkata, West Bengal 700064, India

Accepted 2023 December 7. Received 2023 December 4; in original form 2023 January 28

ABSTRACT

The origin of the diffuse flux of TeV–PeV astrophysical neutrinos is still unknown. The γ -ray blazar PKS 0735+178, located outside the 90 percent localization region at 2.2° from the best-fitting IC-211208A event, was found to be flaring across all wavebands. In addition to leptonic synchrotron (SYN) and SYN self-Compton (SSC) emission, we invoke photohadronic ($p\gamma$) interactions inside the jet to model the spectral energy distribution (SED) and neutrino emission. We analyse the 100 d γ -ray and X-ray data and 10 d around the neutrino event is chosen to generate the broad-band SED. The temporal light curve indicates that the source was in a high state in optical, UV, γ -ray, and X-ray frequencies during the neutrino detection epoch. In the one-zone lepto-hadronic model, the SSC photons do not provide enough seed photons for $p\gamma$ interactions to explain the neutrino event. However, including an external photon field yields a neutrino event rate of 0.12 in 100 d, for the IceCube detector, using physically motivated values of the magnetic field, an external photon field peaking at optical wavelength, and other jet parameters. The radiation from secondary electrons at X-ray energies severely constrains the neutrino flux to a lower value than found in previous studies. Moreover, the flux of high-energy γ -rays at GeV energies from the decay of neutral pions is sub-dominant at the high-energy peak of the SED, suggesting a higher correlation of neutrinos flux with X-ray flux is plausible.

Key words: radiation mechanisms: non-thermal – galaxies: active – galaxies: BL Lacertae objects: individual: PKS 0735+178 – galaxies: jets.

1 INTRODUCTION

The origin of the diffuse flux of astrophysical neutrinos from ~ 10 TeV to a few PeV, detected by IceCube Observatory, is a relatively recent problem in astroparticle physics (IceCube Collaboration 2013, 2014). After 10 yr of their discovery, their sources are still concealed from the eyes of multiwavelength telescopes. Since neutrinos are produced only in hadronic processes, they are smoking gun evidence of cosmic-ray (CR) acceleration inside the source (see e.g. Aartsen et al. 2018a). CRs consist mainly of protons and nuclei and can interact with the ambient matter and radiation fields at the production site and/or during their propagation to Earth. Astrophysical neutrinos are produced along with high-energy photons via photohadronic ($p\gamma$) or hadronuclear (pp) interactions in the source emission region. The magnetic rigidity at tens of PeV energies is insufficient for retaining directional signatures of CRs over cosmological distances. The high-energy universe is opaque to photons beyond a few hundred TeV due to e^+e^- pair production with cosmic background photons. Neutrinos are ideal messengers of CR acceleration because they are weakly interacting, and thus unattenuated by intervening matter or radiation and undeflected by magnetic fields. Thus the discovery of the neutrino emitters will unveil the sources of extragalactic CRs, and even the

ultrahigh-energy CRs (UHECRs; $E > 10^{17}$ eV, see, e.g. Alves Batista et al. 2019; Anchordoqui 2019, for a recent review).

The realtime alert system at the IceCube Neutrino Observatory, located in the South Pole ice, allows rapid follow-up by multiwavelength detectors to search for the source of a high-energy muon-neutrino event (Aartsen et al. 2017a). Neutrinos of astrophysical origin at $\gtrsim 1$ TeV and dec. $\delta \gtrsim 5^\circ$ can be efficiently discriminated from the atmospheric muon contamination with an angular resolution of $< 1^\circ$ for track-like events. Active galactic nuclei (AGNs), powered by accretion on to a supermassive black hole (SMBH), are considered prominent candidates of IceCube astrophysical neutrino signal. The association of the neutrino event IC-170922A with a flaring *Fermi-LAT* blazar TXS 0506+056, at 3σ statistical significance led to the first spatial and temporal correlation of a high-energy ν_μ event with a flaring γ -ray blazar, detected by *Fermi-LAT*, and followed up by several detectors in an intensive multiwavelength campaign (Aartsen et al. 2018b, c). Several other neutrino events are identified thereafter having positional coincidence with blazars but with lower statistical significance (Franckowiak et al. 2020; Giommi et al. 2020).

Blazars are a class of AGN with their collimated beam of outflow pointing towards the observer’s line of sight (Urry & Padovani 1995). These powerful luminous jets are relativistic, extending from pc to kpc scale distances. Blazar jets can provide a suitable environment for CR acceleration and neutrino production (Abbasi et al. 2022).

* E-mail: raj@cft.edu.pl (RP); saikatt@gmail.com (SD)

The blazars with weak or no emission lines are called BL Lacs; they are usually highly variable sources. Based on the frequency of their SYN emission peaks (ν_{peak}) in broad-band spectral energy distribution (SED), BL Lacs are classified into low energy-peaked (LBL) ($\nu_{\text{peak}} \approx 10^{13-14}$ Hz), intermediate energy-peaked (IBL) ($\nu_{\text{peak}} \approx 10^{15-16}$ Hz), and high energy-peaked (HBL) ($\nu_{\text{peak}} \approx 10^{17-18}$ Hz) sources. More recently, the LBLs with peak frequency above $10^{13.5}$ Hz have been named IBL or HBL BL Lacs (Giommi & Padovani 2021). Earlier analyses have shown, however, that a maximum of 30 percent of the cumulative neutrino background can originate from blazars, depending on the scaling relation between γ -rays and neutrinos (Aartsen et al. 2017b).

It is possible that along with electrons, protons are also accelerated to very high energy inside the jet. In the leptonic model, the broad-band SED can be well explained by the SYN and IC emission. It has been noted earlier that in some cases, both leptonic and hadronic models can explain the broad-band SED, and hence a clear detection of neutrino events is required where the hadronic modelling is preferred (Mücke & Protheroe 2001; Böttcher et al. 2013; Petropoulou & Mastichiadis 2014).

In hadronic interactions, the shock-accelerated protons or heavy nuclei interact with the cold protons in the ambient medium (p-p interaction) or low-energy photons (p- γ interaction) and produce the high-energy gamma-rays as well as neutrinos (Böttcher et al. 2013; Reimer, Boettcher & Buson 2019). Although both γ -rays and neutrinos maintain their directionality, due to their non-interacting nature, high-energy neutrinos are the best candidates to probe the acceleration site of CRs and their maximum energy (Eichler 1979; Sikora et al. 1987).

PKS 0735+178 is an IHBL located at a redshift of $z = 0.45 \pm 0.06$ as determined from the detection of its host galaxy (Nilsson et al. 2012). The redshift value of 0.65 has also been suggested in a more recent study by Falomo, Treves & Paiano (2021), but we used 0.45 in this work. During its largest flaring state in 2021 December, it was found to be associated with neutrino events detected by IceCube (IceCube Collaboration 2021), Baikal (Dzhilkibaev, Suvorova & Baikal-GVD Collaboration 2021), Baksan (Petkov et al. 2021), and KM3NeT (Filippini et al. 2022). We have analysed the observational data from *Swift-XRT*, *UVOT*, *NuSTAR*, and *Fermi-LAT* to build the multiwavelength SED during the flaring state. We initially modelled the SED with a leptonic model, which can explain the SED satisfactorily, and subsequently with a lepto-hadronic model to determine whether PKS 0735+178 could be the source of astrophysical neutrinos. An external radiation field, which may originate from the broad line region (BLR), is needed to enhance the neutrino flux. We have discussed the neutrino event detected by the IceCube Collaboration in Section 2 and the analysis of the UV, X-ray, and γ -ray data in Section 3. Our results are presented in Section 4, they are discussed in Section 5, and the conclusions from our results are given in Section 6.

2 NEUTRINO EVENT AND ITS FOLLOW-UP

A GCN circular 31 191 was posted confirming the detection of a high-energy neutrino candidate with a track-like event (IceCube-211208A; IceCube Collaboration 2021). In IceCube, the detection was recorded on 2021-12-08 at 20:02:51.1 UT with a moderate probability of being of astrophysical origin. *Fermi-LAT* reported a significant detection in γ -ray from the blazar PKS 0735+178 (4FGL J0738.1+1742) which was located at ~ 2.2 d $^\circ$ away from the event constructed location by the IceCube (Garrappa et al. 2021b), which triggered a massive search of its counterparts in different wavebands across the globe.

Soon after, many Atels were reported (Carrasco et al. 2021; Feng et al. 2021; Haemmerich et al. 2021; Kadler et al. 2021; Lindfors et al. 2021; Petkov et al. 2021; Savchenko, Larionova & Grisnina 2021). The first broad-band confirmation came from the optical MASTER telescope which reported a brightening in the optical band (Zhirkov et al. 2021) with magnitude 14.1 and soon after the source was observed in a high flux state in γ -ray (Garrappa et al. 2021a), X-ray (Santander & Buson 2021), and radio bands (Kadler et al. 2021). The simultaneous brightening in almost all the electromagnetic regimes during the IceCube detection suggests that this blazar could be the possible source of the neutrino. This motivates us to do a broad-band study to understand the physical mechanism responsible for the broad-band emission and explore the neutrino connection with the blazar.

3 BROAD-BAND OBSERVATIONS AND DATA ANALYSIS

We collected the archival data that is available for this source during this important event and provided a detailed broad-band study including the temporal and spectral properties.

Fermi-LAT

We analysed the Pass8 *Fermi-LAT* data set within energy 100 MeV to 350 GeV of the source 4FGL J0738.1+1742. We use the FERMIPY package developed by Wood et al. (2017) for analysing the *Fermi-LAT* data. A circular 10° region of interest (ROI) was selected around the source for the photons extraction. The events with zenith angle $\theta < 90^\circ$ have been rejected to avoid contamination from the Earth's limb γ -ray. The filter 'gmtktime'(DATA_QUAL>0 && LAT_CONFIG==1) is used to select the good time intervals (GTIs). While analysing the data both the front- and back-type events were considered. The above analysis has been performed with the latest instrument response function (IRF) 'P8R3_SOURCE_V3', isotropic background model 'iso_P8R3_SOURCE_V3_v01' and the galactic diffuse emission model 'gll_iem_v07'. These models can be found on *Fermi* Science Support Center.¹

The LIKELIHOOD analysis provides the test statistics (TS) value of each source within the ROI and for further analysis we reject the sources with low TS (TS < 10). Then we produce the light curve of the interested source keeping its parameters free and by fixing the model parameters of all other sources present within the 10° of the ROI. The upper panel of Fig. 1 shows the weekly binned γ -ray light curve. The source was analysed from 2021 October to 2022 January.

To generate the SED of the sources for modelling, we keep the parameters of the galactic and isotropic diffuse components free, and initially, the parameters of all the other sources present within the ROI are kept fixed. We also reject the sources with a lower TS (TS < 10) value. We calculate flux upper limits in energy bins if the source TS is found to be <9.

The photon index of the target was left free to vary (along with all the other parameters) but that of the other sources was kept fixed. For the background sources that satisfied the TS ≥ 10 limit, only the normalization or pre-factor was left free to vary (depending on the model being power law or LogParabola) whereas their spectral indices were kept fixed. The effect of energy dispersion was acknowledged during the analysis except for 'galdiff' and 'isodiff' for which the effect of energy dispersion was ignored.

¹<https://fermi.gsfc.nasa.gov/ssc/data/access/lat/BackgroundModels.html>

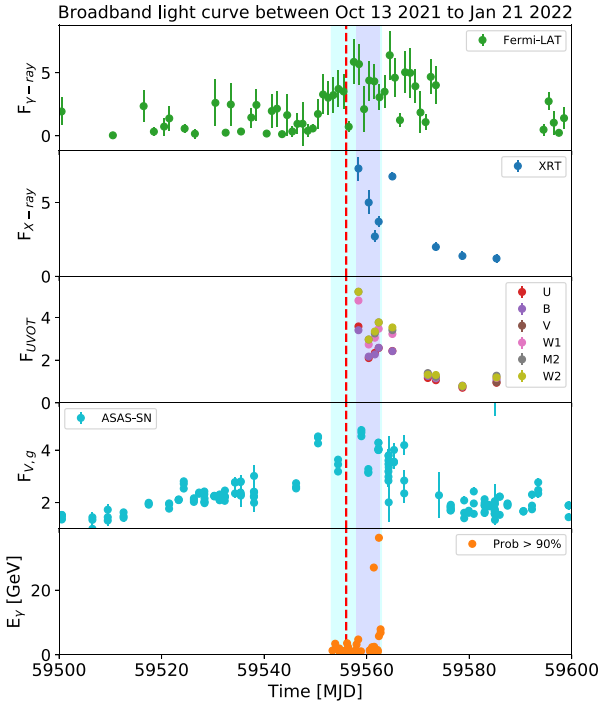


Figure 1. The broad-band light curve for PKS 0735+17. The shaded region is chosen for SED modelling (MJD 59553–59563). The γ -ray data are in units of 10^{-7} ph cm^{-2} s^{-1} , XRT are in 10^{-12} erg cm^{-2} s^{-1} , UVOT are in 10^{-11} erg cm^{-2} s^{-1} , and ASAS-SN are in units of mJy. The big color patch represents the period for γ -ray SED, and the smaller color patch is for X-ray and optical-UV SED.

Swift-XRT

Soon after detecting the neutrino event and the high source activity in γ -ray, the source was proposed for monitoring with *Swift* telescope in X-ray and optical-UV wavebands. We have collected and analysed the long-term data and also focused on the period close to the neutrino event. The analysis is done following the standard *Swift-XRT* procedure. A source and background region of 15 and 30 arcsec is chosen around the source and away from the source to extract their corresponding spectrum. The ancillary response file (ARF) corresponding to each observation is created using the tool XRTMKARF and the corresponding redistribution matrix file (RMF) is obtained from the latest version of the CALDB. The RMFs and ARFs along with the source and background spectrum is loaded into the tool GRPPHA to combine and group them. The final output spectrum of the GRPPHA is binned with 20 counts per bin to achieve the minimum of 20 counts in each bin. The final spectra are loaded into XSPEC and modelled with a simple power-law spectral model. The X-ray photons in the soft energy band are accounted for the galactic correction using the galactic column density, $n_{\text{H}} = 4.5 \times 10^{20}$ cm^{-2} (Willingale et al. 2013).

Swift-UVOT

The advantage of having *Swift* telescope is that it can provide simultaneous observations in optical-UV along with the X-ray. The *Swift* has an ultraviolet optical telescope (UVOT) onboard with six filters namely, *UVV*, *UVU*, *UVB*, *UVW1*, *UVM2*, and *UVW2* where the first three are optical filters and the latter three are ultraviolet. The raw data were analysed following the standard procedure where the source and background region were selected with a circular

region of radius 5 and 15 arcsec around the source and away from the source location, respectively. The magnitude was extracted using the tool UVOTSOURCE from each filter and later was corrected for galactic extinction using the reddening, $E(B - V) = 0.0298$ (Schlafly & Finkbeiner 2011) and extinction ratio corresponding to each wavelength, $A_{\lambda}/E(B - V)$ from Giommi et al. 2006. Further, the corrected magnitude was converted to fluxes using the zero point (Breeveld et al. 2011) and the conversion factors (Poole et al. 2008).

NuSTAR

Following the IceCube event the source was proposed for ToO observation in *NuSTAR* and two observations were done on 2021 December 11 and 2021 December 13 with ~ 22 and ~ 21 ks exposure (Feng et al. 2021). We have analysed these two observations using the standard *NuSTAR* data analysis tool NUSTARDAS 1.9.2 provided by HEASOFT. NPIPELINE was run on both observations to produce the cleaned event file. A circular source and background region were chosen of radius 20 and 40 arcsec, respectively. A tool called NUPRODUCT was run to create the source and background spectra along with corresponding RMFs and ARFs. Further, the spectra were processed in XSPEC.

4 RESULTS

4.1 Broad-band light curves

After the IceCube alert, the source was rigorously monitored across the wavebands. We have shown the temporal behaviour of the source during the event and a few weeks before and after the events to have a clear understanding of its variability. Fig. 1 presents the broad-band light curve over 100 d starting from 1.5 mon before the neutrino event (red dashed vertical line). Before and after the IceCube event the γ -ray flux is low and the detection is not significant in some epochs ($TS < 9$; those data points are removed from the light curve). We noticed that during the neutrino event, the source was rising in γ -rays where the flux rises from $\sim 2 \times 10^{-7}$ to $\sim 6.3 \times 10^{-7}$ ph cm^{-2} s^{-1} within a day. Then it goes down again reaching the flux level $\sim 2 \times 10^{-7}$ ph cm^{-2} s^{-1} within 2 d and again started rising. This confirms a short-term variability in the γ -ray light curve. However, the variability does not coincide exactly with the neutrino event (vertical red line in Fig. 1). Similar behaviour was also seen in the X-ray band where we observed that the source was in a high state (as the later observation suggests) but the observation at the exact IceCube event date was missed in *Swift*. Just after the event, the X-ray observation was done and it showed a clear fast-flux variability (before the events within a few months there were no observations made in X-ray by *Swift-XRT*). The flux goes down by a factor of 3 from 7.3×10^{-12} to 2.7×10^{-12} ergs cm^{-2} s^{-1} just within 3 d after the event and again rises to the high-flux state to 6.76×10^{-12} ergs cm^{-2} s^{-1} within 3 d and then went down to a low-flux state. During this variability, we noticed that the photon spectral index does not change much but we see a slight trend of the ‘softer-when-brighter’. This trend is more clear when plotting all the observations together in Fig. 2. The trend is that of an LBL-type blazar as also seen in Giommi et al. (2021).

Using the 1-d binned γ -ray light curve, we have estimated the flux variability time and the size of the emission region. For that, we followed the expression,

$$F(t_2) = F(t_1) \times 2^{(t_2-t_1)/T_d}. \quad (1)$$

Here, $F(t_1)$ and $F(t_2)$ are the observed fluxes at time t_1 and t_2 , respectively and T_d is the flux doubling/halving time-scale which

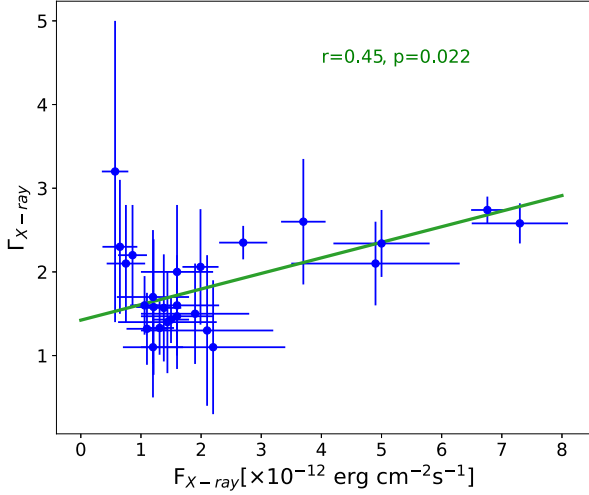


Figure 2. The flux index variation of X-ray emission during the long period. The estimated correlation coefficient (r) is 45 per cent with a null hypothesis probability (p) of 0.02, suggesting a ‘softer-when-brighter’ trend which resembles the LBL-type source (Giommi & Padovani 2021).

means within this time the source flux increases or decreases by a factor of 2. The fastest doubling/halving time in γ -ray was found to be 0.50 ± 0.08 d or 12 h. The hour scale variability is very common in blazars suggesting a compact emitting region. The size of the emission region (R) can be estimated by using the equation,

$$R' = c\delta t_{\text{var}}/(1+z), \quad (2)$$

where R' is estimated to be 2.68×10^{16} cm, using the $\delta = 30$ and $t_{\text{var}} = 0.5$ d, and redshift = 0.45.

Simultaneous to γ -ray and X-ray this source appears to be in a high state also in optical-UV. In UVOT, we do not have any optical-UV observation on the exact date of neutrino detection but the observation done after the event suggests a brightening. We also have access to the long-term ASAS-SN (All-Sky Automated Survey for Supernovae) optical data as shown in panel 4, which confirms the optical brightening during the flaring and the IceCube event. In the lower panel, we show the detection of high-energy photons with probability > 99 per cent. Two high-energy photons of energy above 30 GeV were detected after the IceCube event.

4.2 Multiwavelength SED and neutrino production

Broad-band SED modelling is important to unveil the physical mechanism responsible for broad-band emission and the simultaneous detection of the astrophysical neutrino by IceCube. From the temporal study, it is clear that during the time of neutrino detection, the source was in an active state in γ -ray, X-ray, and optical UV. We have combined the observations from all these wavebands and produced a broad-band SED which we have modelled with a possible lepto-hadronic model.

We start with a pure leptonic scenario, where a distribution of leptons was injected inside the jet. The particle distribution evolved with time and later the SYN and SSC emission was derived. We used a publicly available code, called GAMERA², which solves the

time-dependent transport equation given below,

$$\frac{\partial N(E, t)}{\partial t} = Q(E, t) - \frac{\partial}{\partial E}(b(E, t)N(E, t)) - \frac{N(E, t)}{\tau_{\text{esc}}} \quad (3)$$

where, $Q(E, t)$ is the injected Lepton distribution and $b(E, t)$ corresponds to the energy loss rate by an SYN, SSC, and external Compton (EC) if there is an external radiation field and can be defined as $-dE/dt$. In the last term, we also included the constant escape time $\tau_{\text{esc}} \sim R'/c$, where R' denotes the size of the emitting region and c is the speed of light. The escape of electrons over dynamical time-scales $\tau_{\text{esc}} \sim t_{\text{dyn}} = R'/c$ is a prudent choice and has been widely considered in the literature. This code uses the ‘Klein–Nishina’ cross-section to compute inverse Compton (IC) emission (Blumenthal & Gould 1970). The escape time here represents the time-scale over which adiabatic expansion losses limit the accumulation of relativistic electrons within the source emission region. So, the electrons that escape do not contribute to the observed emission (SYN/IC) any further and are rejected from the system. A quasi-steady state is reached in the emission region when the injection, $Q(E, t)$, is balanced by energy loss and/or escape, which is the ‘cooling’ of the system. The time-dependent transport equation (equation 3) is then used to calculate the electron energy distribution dN/dE in this steady state, which subsequently gives the radiative spectra. Since the source is active simultaneously in all the wavebands and emitting neutrinos, we model the SED using a one-zone emission model. A log-parabola injection spectrum is assumed for electrons and the functional form of the LP distribution is given below,

$$Q(E) = L_0(E/E_0)^{-(\alpha+\beta \log(E/E_0))} \quad (4)$$

where L_0 is the normalization constant, E_0 is the reference energy, and α, β are the spectral index and the curvature parameter. The important thing to note here is that the functional form of the particle spectrum (power law, log-parabola, power law with exponential cut-off, etc.) in jets of blazars is not known. Our choice of the particle spectrum is based on the convenience of fitting the data in our model. One can have a different particle distribution as well.

The CR protons accelerated inside the jet can interact with the soft photons produced in SYN radiation of leptons, thus undergoing various photohadronic processes. The time-scale of these interactions can be expressed as

$$\frac{1}{t'_{p\gamma}} = \frac{c}{2\gamma_p^2} \int_{\epsilon_{\text{th}}/2\gamma_p}^{\infty} d\epsilon'_\gamma \frac{n(\epsilon'_\gamma)}{\epsilon_\gamma^2} \int_{\epsilon_{\text{th}}}^{2\epsilon_\gamma p} d\epsilon_r \sigma(\epsilon_r) K(\epsilon_r) \epsilon_r, \quad (5)$$

where $\sigma(\epsilon_r)$ and $K(\epsilon_r)$ are respectively the cross-section and inelasticity of photopion production or BH pair production as a function of photon energy ϵ_r in the proton rest frame, and $n(\epsilon'_\gamma)$ is the target photon number density (Stecker 1968; Chodorowski, Zdziarski & Sikora 1992; Mücke et al. 2000). Neutrinos and high-energy photons are produced from the decay of charged and neutral pions produced in the photo-pion interactions ($p\gamma \rightarrow p + \pi^0$ or $n + \pi^+$). The decay of π^+ gives secondary leptons ($Q'_{e,\pi}$) and also results in a flux of ν_e and ν_μ . The high energy γ -rays are attenuated beyond TeV energies due to $\gamma\gamma$ pair production with the soft photons produced by the leptons (and also external photons for our EC model). As a result of these interactions, secondary e^\pm s are produced. These secondary leptons along with those from π^+ decay and the e^\pm pair produced in Bethe–Heitler (BH) interactions ($p\gamma \rightarrow p + e^-e^+$) generate secondary cascade emission. The spectrum of high-energy γ -rays from π^0 decay, the spectrum of e^+ and neutrinos from π^+ decay, and the spectrum of secondary e^-e^+ in BH process are estimated following the parametrization in Kelner & Aharonian (2008). All the parametrizations and test cases presented there were reproduced, and

²http://libgamera.github.io/GAMERA/docs/tutorials_main.html

then the proton and photon spectra were modified for our case. This method has been used earlier in many studies, including one of our earlier works (Das, Gupta & Razzaque 2022b).

The high-energy electrons and positrons produced in $\gamma\gamma$ pair production ($Q'_{e,\gamma\gamma}$), charged pion decay ($Q'_{e,\pi}$), and BH process ($Q'_{e,BH}$) can initiate cascade radiation from the jet. We solve the steady-state spectrum of secondary electrons $N'_{e,s}(\gamma_e)$ in the jet frame using the analytical approach of Boettcher et al. (2013), including $Q'_{e,BH}$ in the source term. The escape term is to be the same as primary electrons. In an SYN-dominated cascade, emission from secondary electrons is given by $Q'_s(\epsilon'_s) = A_0 \epsilon'^{-3/2} \int_1^\infty d\gamma'_s N'_{e,s}(\gamma'_s) \gamma_e'^{-2/3} e^{-\epsilon'_s/b\gamma_e'^2}$. At such high energies, the emission of secondary leptons is SYN-dominated due to the suppression of IC efficiency by the Klein–Nishina effect. The flux of escaping high-energy γ -rays from pion decays is given as

$$Q'_{\gamma,esc}(\epsilon'_\gamma) = Q'_{\gamma,\pi}(\epsilon'_\gamma)(1 - \exp(-\tau_{\gamma\gamma}))/\tau_{\gamma\gamma} \quad (6)$$

where, $\tau_{\gamma\gamma}$ is the absorption probability assuming an isotropic photon field, calculated using the formalism given in Gould & Schröder (1967). To increase the efficiency of neutrino production, an escape time-scale of protons longer than the photohadronic interaction time-scale is required (see Fig. 5). Otherwise, the required luminosity in protons increases drastically to obtain a substantial flux of neutrinos (see, e.g. Das, Gupta & Razzaque 2022b). Hence, the energy loss due to proton escape is ignored. The relative weight of the rate of the corresponding process (π production or BH interaction) is applied to the output fluxes. We assume a power-law distribution of protons, extending up to $E_{p,max}$, given by $dN/dE_p \propto E_p^{-\alpha}$, where we consider the same injection spectral index α as for electrons. The normalization of the spectrum is fixed by the kinetic power required in protons to explain the observed SED. The muon neutrino flux at Earth is given as

$$E'_v J'_v = \frac{1}{3} \frac{V' d_B^2 \Gamma^2}{4\pi d_L^2} E'_v Q'_{v,py}, \quad (7)$$

where $Q'_{v,py}$ is the total all-flavour neutrino flux produced in the comoving jet frame. The factor 1/3 approximately takes into account the effect of neutrino oscillations. The $\nu_\mu + \bar{\nu}_\mu$ event rate at IceCube in a given operation time ΔT is calculated using the expression

$$\mathcal{N}'_{\nu_\mu} = \Delta T \int_{\epsilon_{v,min}}^{\epsilon_{v,max}} d\epsilon'_v \frac{d\Phi'_v}{d\epsilon'_v} \langle A_{eff} \rangle_\theta \quad (8)$$

where $\langle A_{eff} \rangle_\theta$ is the effective detector area averaged over the zenith angle bin concerned (Aartsen et al. 2019). We use the effective area for event selection as a function of neutrino energy from Stettner (2020). The all-flavour neutrino flux can be approximated as three times the muon neutrino flux.

The IR optical-UV and soft-X-ray emissions from PKS 0735+178 are expected to be produced by the SYN emission of relativistic leptons in a strong magnetic field. However, the hard X-ray and γ -ray are expected to be produced by the SSC process. In our analysis, although the X-ray data corresponds to 10 d around the time of flaring, we consider a steady proton injection, and hence the electromagnetic cascade and neutrino fluxes correspond to that produced in the flaring state once a steady state is reached as shown on the left panels of Figs 3 and 4. The multiwavelength SED models obtained by using a pure leptonic and a lepto-hadronic emission model are shown in the left and right panels of Fig. 3. The best-modelled parameters are shown in Table 1. The X-ray flux at keV energies provides stringent constraints on the secondary cascade emission and hence, limits the neutrino flux. We vary the proton maximum energy $E'_{p,max}$ in logarithmic intervals between 0.1 and 10 PeV to find the best model

to SED and simultaneously maximize the neutrino flux. A steep cut-off in the proton spectrum is required to explain the observed neutrino event. Extending the proton spectrum to higher energies shifts the neutrino peak to higher energies. Hence a cut-off to the spectrum is required at $\gamma'_{p,max}$ in our modelling. The neutrino flux peaks at ~ 0.1 PeV. However, the luminosity requirement is very high in this case, much above the Eddington limit.

4.3 With external photon field

Since the source is argued to be a ‘masquerading BL Lac,’ it can also have an external radiation field, such as a BLR and the dusty molecular torus. In the modelling, we consider that the emission region is within the boundary of the BLR, and hence, the radiation field from BLR will dominate the emission in γ -ray and the neutrino event flux. As argued in Ghisellini et al. (2011) the transition line between BL Lac and FSRQ (Flat Spectrum Radio Quasar) type object can be given by the ratio of BLR luminosity to Eddington luminosity, $L_{BLR}/L_{Edd} \sim 5 \times 10^{-4}$. Considering the black hole mass as $\sim 10^9 M_\odot$, the Eddington luminosity is estimated as 1.26×10^{47} erg s $^{-1}$ which lead to the $L_{BLR} = 6.3 \times 10^{43}$ erg s $^{-1}$. Because a very small portion of the disc photon gets reprocessed in BLR (10 per cent), the disc luminosity can be derived as $L_{disc} = 6.3 \times 10^{44}$ erg s $^{-1}$. The BLR energy density in the comoving frame can be estimated using the expression

$$U'_{BLR} = \frac{\Gamma^2 L_{BLR}}{4\pi R_{BLR}^2 c}, \quad (9)$$

where, $R_{BLR} \sim 10^{17} L_{disk,45}^{0.5}$. Using the above values of L_{BLR} and L_{disc} , the size of the BLR and BLR energy density is estimated as, $R_{BLR} = 0.79 \times 10^{17}$ cm and $U'_{BLR} = 23.88$ erg cm $^{-3}$, respectively. Please note that due to the uncertainties in the scaling relation, these values are correct within a factor of a few. We also derive the location of the emission region down the jet using an expression, $d \sim 2c\Gamma^2 t_{var}/(1+z) \sim 2.33 \times 10^{18}$ cm, which suggests that the emission region is located at the outer boundary of the BLR. The BLR photon density sharply drops with increasing distance from the BLR (Ghisellini & Tavecchio 2009) and therefore the estimated value for U'_{BLR} from the modelling is less than this value (Table 1). The size of the emission region in both cases is optimized during the modelling and is found to be less than what is expected from the variability estimation in equation (2).

5 DISCUSSIONS

Neutrinos from astrophysical phenomenon is a smoking-gun evidence of CR acceleration. The identification of the sources of IceCube detected diffuse astrophysical neutrino flux is of paramount importance to unveil extreme high-energy processes. Blazars are a potential candidate, among others, for neutrino emission through hadronic processes in their relativistic jets. Several sources have been identified in spatial coincidence with IceCube muon tracks. TXS 0506+056 is the only source associated spatially and temporally during the flaring activity in the *Fermi-LAT* waveband, with a ν_μ event at the IceCube. However, the blazar PKS 0735+178 provides a testbed of one more such association. This BL Lac object lies within 90 per cent error region of one track-like event at IceCube of energy $E'_v = 172$ TeV. It can also be associated with a larger error region of a cascade event at the Baikal observatory of energy 43 TeV (Dzhilkibaev & Suvorova 2022), and an 18 TeV neutrino detected by KM3NeT (Filippini 2022).

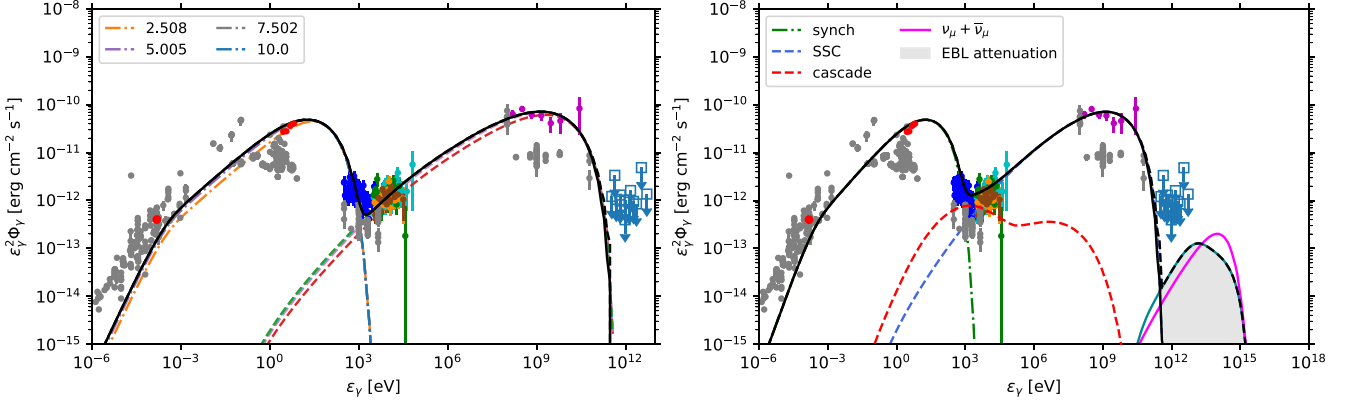


Figure 3. Broad-band SED model obtained for only SYN and SSC emission with no external photon field. Red data points are UVOT, blue are XRT, green and orange are *NuSTAR* (FPMA and FPMB), and magenta is GeV data from *Fermi-LAT*. The grey data points are the archival data. The left panel shows the purely leptonic emission case. Here, the different line styles (shown in the legend for the SYN spectrum) correspond to the time evolution of the SED for a period of 10 d. The right panel shows the SED including $p\gamma$ interactions on the steady-state leptonic SED. The red dashed curve shows the secondary cascade radiation. The final spectrum is corrected for $\gamma\gamma$ pair production inside the jet and attenuation in the EBL (grey-shaded region). The magenta line is the muon neutrino flux obtained in this model for the best-fitting proton maximum energy. The SEDs are produced for the marked period in Fig. 1 for MJD 59553–59563 (2021-12-05 to 2021-12-15). We also include the radio flux at 37 GHz shown in red colour (Kadler et al. 2021; Acharyya et al. 2023).

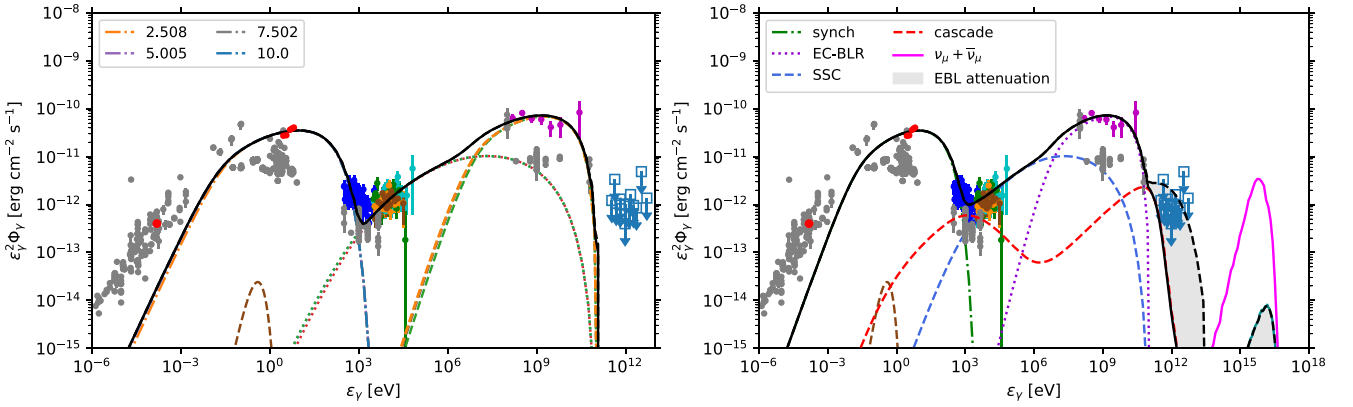


Figure 4. Broad-band SED modelled using SYN and IC emission off an external radiation field. The colours are the same as in Fig. 3. The left panel shows the purely leptonic emission case. The different line styles (shown in the legend for the SYN spectrum) correspond to the time evolution of the SED over a period of 10 d. The right panel shows the SED including $p\gamma$ interactions on the steady-state leptonic SED and also on the external black body radiation field (dashed brown). The red dashed curve shows the secondary cascade radiation. The final spectrum is corrected for $\gamma\gamma$ pair production over all the available radiation fields in the jet emission region and attenuation in the EBL (grey-shaded region). The magenta line is the muon neutrino flux obtained in this model for the best-fitting proton maximum energy. We also include the radio flux at 37 GHz (Kadler et al. 2021) shown in red square and the VHE data points from the VERITAS are shown for the comparison purpose in blue square (Acharyya et al. 2023).

In this article, we have studied the long-term γ -ray, X-ray, and UV optical data of the source. The SED reveals an active state during the IceCube detection epoch. The γ -ray and X-ray light curve exhibits a day-scale variability where the flux varies by a factor of ~ 3 in the high state in comparison to the low state. In our one-zone lepto-hadronic modelling, we consider two cases viz., with and without external photon field. The absence of spectral emission lines suggests the source to be a BL Lac. However, the SSC spectrum provides insufficient target photons for neutrino production. The neutrino flux peaks at ≈ 0.1 PeV and the corresponding flux value is $\sim 2 \times 10^{-13}$ erg cm 2 s $^{-1}$. For higher values of $E'_{p,\max}$, the Bethe-Heitler cascade increases near the X-ray energies, hindering the increase in neutrino flux due to the restriction from *Swift* data. It should be noted, that the required kinetic power in protons exceeds the Eddington luminosity of the source by more than two orders of magnitude. We have checked that for protons to interact dominantly

with the SYN photons, $E'_{p,\max}$ must be $\gtrsim 10^{17}$ eV, and hence $\Gamma E'_{p,\max}$ corresponds to ultrahigh energies, which may lead to signatures of the extragalactic cascade at multi-TeV energies (Das, Razaque & Gupta 2022a). In the absence of \sim TeV photon detection, such a scenario is possible but contentious. Hence, for more reasonable results, PKS 0735+178 can be considered a ‘masquerading BL Lac’ similar to TXS 0506+056, with hidden emission lines (Padovani et al. 2019). The external photons from the BLR region are then used as the primary target for $p\gamma$ interactions, producing a detectable neutrino flux.

In our work, we consider an external photon field of temperature 5×10^4 K, i.e. within the optical frequency range. The X-ray data severely restricts the flux of SYN radiation from secondary electrons. The cascade flux in turn limits the allowed neutrino flux level. The neutrino event rate in our study is found to be 1.3×10^{-8} events per second. The expected events rate during the current high state

Table 1. Multiwavelength SED modelling results with the values of the best-model parameters. The Doppler factor and the Lorentz factor are fixed at 30.0 considering $\delta \sim \Gamma$. The redshift of the source is fixed at 0.45.

Parameters	SSC	SSC + EC
δ_D	30	30
B' [Gauss]	0.55	4.5
R' [cm]	7.0×10^{15}	2.0×10^{15}
α (elp spectral index)	1.90	1.60
β (log parabola curvature)	0.04	0.001
E_0 [GeV]	0.09	0.1
$\gamma'_{e,\min}$	30	100
$\gamma'_{e,\max}$	3.1×10^4	1.0×10^4
U'_{BLR} [erg cm $^{-3}$]	–	1.9
T'_{BLR} [K]	–	5.0×10^4
$\gamma'_{p,\min}$	10.66	10.66
$\gamma'_{p,\max}$	1.7×10^5	4.26×10^6
$L_{j,e}$ [erg s $^{-1}$]	1.52×10^{47}	2.79×10^{44}
$L_{j,B}$ [erg s $^{-1}$]	0.1×10^{45}	6.8×10^{45}
$L_{j,p}$ [erg s $^{-1}$]	6.3×10^{49}	6.3×10^{47}

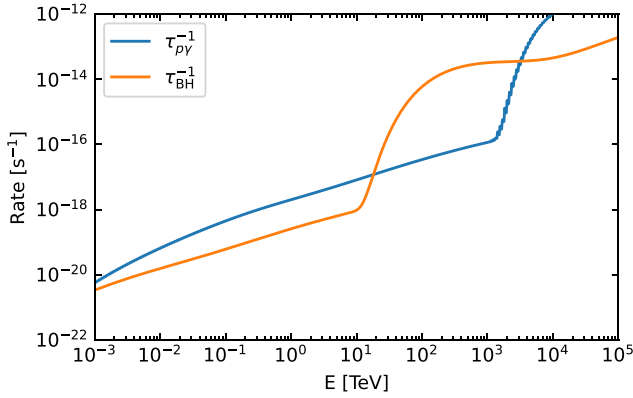


Figure 5. A comparison of the rates of photopion interactions and Bethe–Heitler pair production processes.

of the source is ~ 0.12 events per 100 d. Overall, the fit to the observed SED is significantly improved compared to the SSC model. A higher neutrino flux can be achieved if the peak of the external photon spectrum is further blue shifted. However, we have limited the photon field within the optical range, as considered widely in the literature for TXS 0506+056 (Keivani et al. 2018). Also, we emphasize the fact that an updated and detailed study of the X-ray flux and a fit to the archival radio data provide limited flexibility of the jet parameters. However, it should be noted that both the SSC model and the EC model require the proton spectrum to be cut-off steeply at a specific energy, which is difficult to explain. One possibility is that, at higher energies, the cooling time-scale may become shorter than the acceleration time-scale or the acceleration process may become inefficient at higher energies reaching the limits in the physical size of the acceleration region. In a recent work by Acharyya et al. (2023), they modelled the broad-band SED including VERITAS (Very Energetic Radiation Imaging Telescope Array System) and HESS (High Energy Stereoscopic System) SED data points with SSC, EC, and lepto-hadronic model. They predict the nominal neutrino flux at 170 TeV is 1.5 neutrinos per year (or

0.125 neutrinos per month) using an effective area of 30 m 2 which is a bit higher than our case.

As shown in Table 1, the maximum energy of electrons and the protons differ very much which is because the electrons are rapidly cooled due to radiative losses and are difficult to accelerate to energies beyond sub-TeV energies. While protons are less efficient in radiation loss, and $\sim 2 \times 10^3$ heavier than electrons, differing in the rest-mass energy by the same factor. Hence, it will be more reasonable to compare their Lorentz factors and not energies for relativistic processes. From a modelling perspective, the energy transferred to neutrinos via the photopion interaction process is $E_\nu \approx E_p/20$. Hence to obtain a neutrino of energy ~ 0.2 PeV, the required proton maximum energy must be $E_{p,\max} \approx 4$ PeV in the observer frame, which corresponds to $E'_{p,\max} = (1+z)E_{p,\max}/\Gamma \approx 0.2$ PeV in the comoving jet frame. However, the neutrino flux in our modelling peaks at a few PeV in the observer frame, requiring higher maximum proton energy. This is still within the energy uncertainty of the neutrino observation (Acharyya et al. 2023; Sahakyan et al. 2023).

We find the X-ray-neutrino correlation is more probable than the γ -neutrino correlation in the case of this source. A similar conclusion can be found for the TXS 0506+056 blazar in the literature (Keivani et al. 2018), in which case too the pion decay cascade is sub-dominant at the VHE γ -ray domain. However, the neutrino flux upper limit estimated by IceCube for 0.5 or 7.5-yr averaged observation of one event like IC-170922A is much higher than that obtained here. The IceCube detection potential is not sensitive to the flux level obtained here. Also, for the cascade event detection by Baikal, the angular uncertainty of positional correlation is poor, $\sim 5.5^\circ$. In that case, one cannot ignore the possibility that other blazar sources within the 50 per cent containment zone can also be the possible source. However, for neutrino multiplets from this source, the estimated neutrino flux is more than an order of magnitude higher than that obtained here. Such high neutrino fluxes are extremely difficult to produce in a flare time of 21 d (comparing with Sahakyan et al. 2023), and one needs to invoke a hidden sector of neutrino production, or multiple zones, or neutrino production in the vicinity of the SMBH, outside the jet region.

The broad-band SED of PKS 0735+178 has been modelled in a recent study by Sahakyan et al. (2023) where they have used a lepto-hadronic model and considered the three possible scenarios namely $p\gamma$ with proton-SYN, SSC and with EC. In p -SYN the model demands a very high magnetic field of the order of 100 Gauss, which is debatable in blazars. Their hybrid model with SSC required a very high proton luminosity exceeding the Eddington luminosity of the source. They also considered the external photon field to explain the high energy γ -ray and eventually for the p - γ interactions to explain the observed neutrino event. They found a neutrino event rate of 0.067 neutrinos per 21 days which corresponds to 0.3 neutrinos in 100 days. However, the constraints from X-ray flux are not considered there. Their external photon field has a luminosity of $L_{\text{BLR}} = 2 \times 10^{43}$ erg s $^{-1}$, which peaks at 2×10^{15} Hz (i.e. 8.3 eV).

In our modelling, we noticed that the SSC model requires much higher jet power than the Eddington luminosity, which motivated us to include an external photon field. Even after including the external photon field the required jet power is higher than the Eddington luminosity. As mentioned earlier, in our model the external photon field peaks at the optical frequency and the jet luminosity required is 6.3×10^{47} erg sec $^{-1}$, which is a factor of few higher than the Eddington luminosity of this source $L_{\text{Edd}} = 1.2 \times 10^{46} (M_{\text{BH}}/10^8 M_\odot)$ erg sec $^{-1}$, where M_\odot is the Solar mass. The mass of the black

hole $M_{BH} \sim 10^{8.8 \pm 0.4} M_{\odot}$ has been assumed following Labita et al. (2006). Our estimated proton jet power is similar to Sahakyan et al. (2023). The jet power in injected electrons obtained by other authors in blazar modelling varies within a range depending on the flare data and the model used to fit the data. The modelling done by Acharyya et al. (2023) predicts a total jet power of 2.0×10^{48} erg s⁻¹, and a lower jet power is predicted for a harder proton spectrum, which is similar to our result.

6 CONCLUSIONS

The modelling of multiwavelength emission from jetted AGNs requires the knowledge of apparent jet speeds and their adiabatic evolution, the magnetic field, size, and distance of emission region, etc. However, neutrino emission is a direct probe of CR acceleration despite the degeneracy in these model parameters and depends dominantly on the available target photons for photopion production, providing essential constraints to blazar properties. In the case of BL Lac objects, neutrino production is suppressed in a one-zone photohadronic model due to the lack of sufficient target photons from SSC. In this work, we have studied a recent association of γ -ray blazar PKS 0735+178 with an IceCube muon track detected on 2021 December, without invoking any exotic physical phenomenon. We predict the resulting neutrino fluxes, aided by a multiwavelength SED model obtained in various scenarios, with and without an external blackbody radiation field. The obtained flux levels are still much lower than the IceCube operation sensitivity. Resolving the uncertainty around the temperature and density of these external seed photons for photohadronic processes is a non-trivial task, and we restrict ourselves to optimal values found in the literature. Interestingly, an association between the X-ray flux and neutrino emission is irrefutable. We conclude that the blazar's contribution to the diffuse neutrino background cannot be neglected. Upcoming detectors with improved sensitivity and angular resolution will be able to pinpoint the neutrino-emitting blazars and constrain our neutrino flux predictions.

ACKNOWLEDGEMENTS

We thank the anonymous referee for insightful comments and suggestions which have helped to improve the scientific clarity of our work. RP and BZ are grateful for the support of the Polish Funding Agency National Science Centre, project 2017/26/A/ST9/00756 (MAESTRO 9) and the European Research Council (ERC) under the European Union's Horizon 2020 research and innovation programme (grant agreement number 951549). The work of SD was supported by JSPS KAKENHI grant number 20H05852. Numerical computation in this work was partly carried out at the Yukawa Institute Computer Facility.

DATA AVAILABILITY

All the data are publicly available and can be accessed easily.

REFERENCES

Aartsen M. G. et al., 2017a, *Astropart. Phys.*, 92, 30
Aartsen M. G. et al., 2017b, *Astrophys. J.*, 835, 45
Aartsen M. G. et al., 2018a, *Adv. Space Res.*, 62, 2902
Aartsen M. G. et al., 2018b, *Science*, 361, 147
Aartsen M. G. et al., 2018c, *Science*, 361, eaat1378
Aartsen M. G. et al., 2019, *Eur. Phys. J. C*, 79, 234

Abbasi R. et al., 2022, *ApJ*, 938, 38
Acharyya A. et al., 2023, *ApJ*, 954, 70
Alves Batista R. et al., 2019, *Front. Astron. Space Sci.*, 6, 23
Anchordoqui L. A., 2019, *Phys. Rept.*, 801, 1
Blumenthal G. R., Gould R. J., 1970, *Rev. Mod. Phys.*, 42, 237
Boettcher M., Reimer A., Sweeney K., Prakash A., 2013, *ApJ*, 768, 54
Breeveld A. A., Landsman W., Holland S. T., Roming P., Kuin N. P. M., Page M. J., 2011, in McEnery J. E., Racusin J. L., Gehrels N.eds, AIP Conf. Ser. Vol. 1358, Gamma Ray Bursts 2010. AIP, Melville, NY, p. 373
Böttcher M., Reimer A., Sweeney K., Prakash A., 2013, *ApJ*, 768, 54
Carrasco L., Recillas E., Escobedo G., Porras A., Chavushyan V., Mayya Y. D., 2021, ATel, 15148, 1
Chodorowski M. J., Zdziarski A. A., Sikora M., 1992, *ApJ*, 400, 181
Das S., Razaque S., Gupta N., 2022a, *A&A*, 658, L6
Das S., Gupta N., Razaque S., 2022b, *A&A*, 668, A146
Dzhilkibaev Z. A., Suvorova O., 2022, ATel, 15112
Dzhilkibaev Z. A., Suvorova O., *Baikal-GVD Collaboration*, 2021, ATel, 15112, 1
Eichler D., 1979, *ApJ*, 232, 106
Falomo R., Treves A., Paiano S., 2021, ATel, 15132, 1
Feng Q., Jin W., Mori K., Mukherjee R., Santander M., Woo J., 2021, ATel, 15113, 1
Filippini F., 2022, ATel, 15290
Filippini F. et al., 2022, ATel, 15290, 1
Frankowiak A. et al., 2020, *ApJ*, 893, 162
Garrappa S., Buson S., Sinapius J., Kadl M., 2021a, ATel, 15099, 1
Garrappa S., Buson S., Sinapius J., Kadler M., *Fermi-LAT Collaboration*, 2021b, GRB Coordinates Network, 31194, 1
Ghisellini G., Tavecchio F., 2009, *MNRAS*, 397, 985
Ghisellini G., Tavecchio F., Foschini L., Ghirlanda G., 2011, *MNRAS*, 414, 2674
Giommi P., Padovani P., 2021, *Universe*, 7, 492
Giommi P. et al., 2006, *A&A*, 456, 911
Giommi P., Glauch T., Padovani P., Resconi E., Turcati A., Chang Y. L., 2020, *MNRAS*, 497, 865
Giommi P. et al., 2021, *MNRAS*, 507, 5690
Gould R. J., Schröder G. P., 1967, *Phys. Rev.*, 155, 1404
Haemmerich S., Zainab A., Gokus A., Weber P., Kreykenbohm I., Wilms J., 2021, ATel, 15108, 1
IceCube Collaboration, 2013, *Science*, 342, 1242856
IceCube Collaboration, 2014, *Phys. Rev. Lett.*, 113, 101101
IceCube Collaboration, 2021, GRB Coordinates Network, 31191, 1
Kadler M. et al., 2021, ATel, 15105, 1
Keivani A. et al., 2018, *ApJ*, 864, 84
Kelner S. R., Aharonian F. A., 2008, *Phys. Rev. D*, 78, 034013
Labita M., Treves A., Falomo R., Uslenghi M., 2006, *MNRAS*, 373, 551
Lindfors E. et al., 2021, ATel, 15136, 1
Mücke A., Protheroe R. J., 2001, *Astropart. Phys.*, 15, 121
Mücke A., Engel R., Rachen J. P., Protheroe R. J., Stanev T., 2000, *Comput. Phys. Commun.*, 124, 290
Nilsson K., Pursimo T., Villforth C., Lindfors E., Takalo L. O., Sillanpää A., 2012, *A&A*, 547, A1
Padovani P., Oikonomou F., Petropoulou M., Giommi P., Resconi E., 2019, *MNRAS*, 484, L104
Petkov V. B., Novoseltsev Y. F., Novoseltseva R. V., *Baksan Underground Scintillation Telescope Group*, 2021, ATel, 15143, 1
Petropoulou M., Mastichiadis A., 2014, *MNRAS*, 447, 36
Poole T. S. et al., 2008, *MNRAS*, 383, 627
Reimer A., Boettcher M., Buson S., 2019, *ApJ*, 881, 46
Sahakyan N., Giommi P., Padovani P., Petropoulou M., Bégué D., Boccardi B., Gasparyan S., 2023, *MNRAS*, 519, 1396
Santander M., Buson S., 2021, ATel, 15102, 1
Savchenko S. S., Larionova E. G., Grismina T. S., 2021, ATel, 15021, 1
Schlafly E. F., Finkbeiner D. P., 2011, *ApJ*, 737, 103
Sikora M., Kirk J. G., Begelman M. C., Schneider P., 1987, *ApJ*, 320, L81
Stecker F. W., 1968, *Phys. Rev. Lett.*, 21, 1016
Stettner J., 2020, *PoS, ICRC2019*, 1017
Urry C. M., Padovani P., 1995, *PASP*, 107, 803

Willingale R., Starling R. L. C., Beardmore A. P., Tanvir N. R., O'Brien P. T., 2013, *MNRAS*, 431, 394

Wood M., Caputo R., Charles E., Di Mauro M., Magill J., Perkins J. S., *Fermi-LAT Collaboration*, 2017, in 35th International Cosmic Ray Conference (ICRC2017). p. 824

Zhirkov K. et al., 2021, ATel, 15098, 1

This paper has been typeset from a $\text{\TeX}/\text{\LaTeX}$ file prepared by the author.